Research Square

Preprints are preliminary reports that have not undergone peer review.
They should not be considered conclusive, used to inform clinical practice,
or referenced by the media as validated information.

Research on a Fault Fast Self-Healing Method Based on Distributed Energy Storage Cluster Control Strategy

Chuan Zhou

zhouchuan@tju.edu.cn

Tianjin University

Suying Gui

Jiangxi Agricultural University

Yongtao Ma

Tianjin University

Research Article

Keywords:

Posted Date: November 23rd, 2026

DOI: https://doi.org/10.21203/rs.3.rs-11576513/v1

License: This work is licensed under a Creative Commons Attribution 4.0 International License.
Read Full License

Additional Declarations: No competing interests reported.

Research on a Fault Fast Self-Healing Method Based on Distributed Energy Storage Cluster Control Strategy

Zhouchuan[1]* , Gui Suying [2] , Ma Yongtao[1]
1. School of Microelectronics, Tianjin University;
2. School of Software, Jiangxi Agricultural University
Corresponding Author: Zhouchuan
Corresponding author(s). E-mail(s): zhouchuan@tju.edu.cn

Abstract： To address the fault self-healing bottlenecks in active distribution networks (ADNs) with high-penetration distributed energy resources, this paper proposes a fast fault self-healing method based on distributed energy storage (DES) cluster cooperative control. The integrated framework combines voltage cooperative control and mode-adaptive frequency deviation control to enhance the operational stability and fault resilience of ADNs under both grid-connected and post-fault islanded scenarios.The voltage cooperative control strategy is functional for both grid-connected and islanded operation, while the frequency deviation control is triggered only upon feeder islanding to prevent unnecessary control intervention during normal grid operation. To achieve high-precision voltage regulation, an enhanced droop-based cooperative control approach is developed by fully considering the residual capacity of individual DES units and the inherent impedance characteristics of distribution feeders. Meanwhile, droop coefficient tuning principles are formulated to coordinate the dynamic responses of multiple DES units. This design effectively suppresses feeder-wide voltage fluctuations in grid-connected mode and maintains stable voltage profiles under islanded operating conditions.For islanded frequency regulation, a dual-hysteresis frequency control strategy is presented to improve the post-fault frequency support performance of DES clusters. Equipped with bidirectional upper and lower hysteresis comparison mechanisms, the proposed scheme accurately identifies positive and negative frequency deviations and enables DES frequency regulation loops according to preset thresholds. This strategy achieves reliable frequency restoration and precise islanding detection without relying on communication links, and it exhibits superior robustness against stochastic frequency disturbances induced by real-time power fluctuations during grid-connected operation.A distinct advantage of the proposed DES cluster control strategy is its full communication independence, which eliminates data interaction and information sharing among feeder nodes. Only local voltage and frequency measurements are utilized to implement

cooperative voltage regulation for grid-connected operation and adaptive frequency stabilization for islanded operation. Integrating with feeder reclosing and automatic transfer switching technologies, the proposed method enables rapid feeder reconfiguration and efficient fault self-healing, offering a practical and effective solution for improving the operational resilience of modern active distribution networks.

0 Introduction

The high penetration of intermittent distributed generation (DG) fundamentally alters the power flow and fault response characteristics of active distribution networks, making fault self-healing a core capability for improving grid operational resilience and power supply reliability. This field has attracted extensive research attention in recent years. Existing studies have primarily focused on post-fault island partitioning, islanded operational stabilization, and load restoration. Typical solutions include heuristic search, intelligent optimization algorithms, and interval power flow-based topological reconfiguration, which effectively optimize island partitioning schemes and maximize restored load capacity under predefined constraints [1-5]. Nevertheless, most existing methods rely solely on static network topology optimization and ignore the dynamic voltage and frequency stability regulation requirements during sudden unplanned feeder islanding, which severely restricts the self-healing reliability of practical DG-dominated distribution systems.

In terms of control architecture, existing distribution network self-healing systems are categorized into centralized, distributed, and hybrid frameworks [6-9]. Centralized architectures achieve near-global optimal restoration via unified global information scheduling and centralized decision-making, yet they suffer from poor anti-interference capability and high failure risks due to heavy reliance on communication infrastructure [10,11]. Traditional distributed architectures improve operational autonomy through peer-to-peer local interaction, but limited local measurement information restricts multi-resource cooperative regulation, resulting in suboptimal restoration performance [12-14]. Emerging hybrid schemes integrate centralized decision advantages and distributed execution flexibility, but they still require real-time data interaction and cannot support fully communication-independent operation, which limits their deployment in complex communication-constrained distribution scenarios [15-17]. Accordingly, a communication-free distributed cooperative self-healing architecture is urgently needed for resilient active distribution

network operation.

A complete distribution network fault self-healing process comprises fault isolation, islanding detection, islanded stability control, and service restoration [18-20]. Fault isolation blocks fault propagation within milliseconds, providing a prerequisite for subsequent self-healing procedures. Islanding detection serves as a critical trigger for post-fault stability control and restoration [21-23]. Current research prioritizes the topological feasibility of island partitioning while neglecting dynamic operational stability after unplanned islanding. Most existing stability control strategies target planned islanding scenarios and fail to address the severe voltage and frequency fluctuations induced by DG stochastic power fluctuations in sudden islanding events [24-26]. In addition, conventional restoration schemes based on reclosing and automatic transfer switching lack coordinated flexible resource regulation, easily causing secondary power shocks during grid reconnection and restricting self-healing accuracy and speed [27-30]. In summary, the absence of adaptive voltage–frequency cooperative control and communication-free self-healing solutions for unplanned feeder islanding is the key research gap addressed in this work.

Targeting the aforementioned research gaps, this paper proposes a fully communication-free fast fault self-healing method based on distributed energy storage (DES) cluster cooperative control for high-DG-penetration active distribution networks, which adapts to unplanned feeder islanding scenarios. Different from conventional topology-reconfiguration-based self-healing methods, the proposed dual-mode control framework integrates an improved droop-based voltage coordination strategy and a novel dual-hysteresis frequency deviation control strategy to realize adaptive grid-connected/islanded mode switching. The improved droop control optimizes coefficient tuning by jointly considering DES residual capacity and feeder impedance, which effectively suppresses feeder-wide voltage fluctuations during normal grid-connected operation. The specially designed dual-hysteresis frequency control is activated only under islanded conditions, achieving precise islanding identification and directional frequency correction without any inter-node information exchange. By utilizing only local voltage and frequency measurements, DES clusters autonomously maintain post-fault island stability and cooperate with reclosing and automatic transfer switching to realize low-shock, rapid feeder restoration. Equipped with a fully communication-independent distributed architecture, the proposed strategy exhibits prominent robustness and adaptability for complex and communication-constrained distribution scenarios. Real-time digital simulation

(RTDS) results verify the superiority and feasibility of the proposed method, providing a practical solution for improving the fault self-healing capability and operational resilience of modern active distribution networks.

1. Voltage Coordinated Control Method for Grid-Connected and Islanded Operation Based on Improved Droop Control

The typical topology of distribution networks is radial, with feeders serving as critical components for power distribution. In conventional feeders, power flow is unidirectional. However, with high penetration of distributed generation (DG), power flow in modern distribution feeders may become bidirectional, feeding into or out of different branches. A representative feeder topology with distributed energy storage (DES) integration is shown in Fig. 1. DES units, loads, and DG units are connected to different feeder nodes through a common transformer. Circuit breakers are installed at both ends of each feeder segment to enable fast fault isolation via relay protection.

Depending on the fault locations (denoted as K2, K3, and K4), fault isolation may result in the formation of distinct islands, e.g., Region 1, Region 2, and Region 3. If the fault is transient, these islands can be reconnected to the main grid through automatic reclosing. For permanent faults, feeder reconnection can be achieved by closing transfer circuit breakers to restore power to the affected segments.

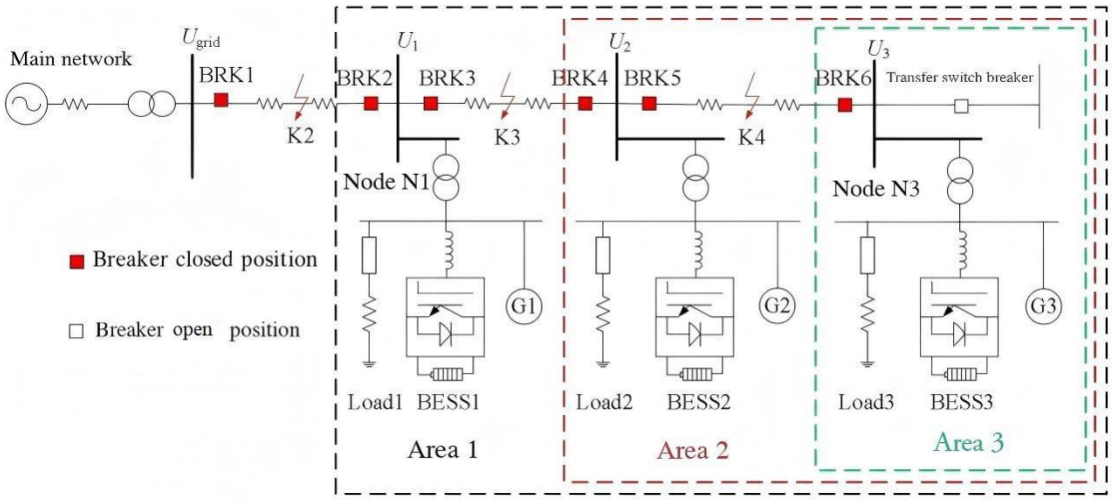

Figure 1. Topology of a distribution network with integrated distributed energy storage (DES)

1.1 Droop Coefficient Setting Method for Distributed Energy Storage

Considering Storage Capacity and Line Impedance

In distribution feeders with high penetration of distributed generation, distributed energy storage (DES) units can effectively suppress voltage violations and enhance the orderly operation of islanded feeders due to their fast and flexible regulation capabilities. By deploying small-capacity DES units at different feeder nodes and employing cluster-based coordinated control, local power compensation at each node can be achieved, thereby stabilizing voltage across the entire feeder. When feeder faults result in islanding, DES units collaboratively regulate islanded voltage and frequency, supporting successful reclosing or automatic transfer switching to ensure continuous power supply.

The key to achieving these functions is coordinating the dynamic output of multiple DES units under both grid-connected and islanded conditions, so that active and reactive power injections follow a unified logic, avoiding mutual cancellation and fully exploiting the cluster control capability. In practical engineering applications, master–slave centralized control architectures are often used for coordination. However, due to cost and communication constraints, some distribution feeders cannot be equipped with sufficient communication support.

To address limited communication conditions, this paper proposes a fully distributed voltage coordinated control method for DES based on an improved droop control strategy. According to the voltage distribution characteristics of the feeder, the product of DES output current and droop slope is added to the rated voltage to form a new voltage reference, which is then input to the voltage controller. By appropriately setting the droop slope, real-time coordinated allocation of active and reactive power among multiple DES units can be realized. Under grid-connected operation, this method enables coordinated voltage regulation at all feeder nodes. When the feeder is islanded, no control strategy switching is required, and voltage stability is still maintained.

Compared with existing droop control methods for DC microgrids, this approach redefines the droop slope calculation for AC feeders, overcoming the control complexity caused by AC line impedance and active–reactive power coupling, and achieving communication-independent voltage coordination and islanded support. The DES voltage droop control method requires the introduction of droop slopes in the voltage control loop, as expressed in Equation (1).

$$U^{*}_{\text{ref_pu}} = U_{\text{ref_pu}} - k \cdot I_{\text{bess_pu}} \tag{1}$$

Here, $I_{\text{BESS_pu}}$ denotes the per-unit value of the DES current, with the convention that current flowing into the bus is negative and current flowing out of the bus is positive (note: the per-unit base is the rated capacity of the DES). U_{ref} is the per-unit reference voltage based on the rated voltage, and U_{ref}^{*} represents the actual DES reference voltage after introducing the droop slope. k denotes the droop slope.

For analytical convenience, the voltage distribution is examined on a feeder with two nodes. The load and generation at each node are equivalently represented as a single total load. Assuming the total load current flows out from the bus, the DES current is directed opposite to the load current to compensate for voltage drops caused by the load. The two-node feeder system can thus be equivalently represented by the circuit shown in Fig. 2.

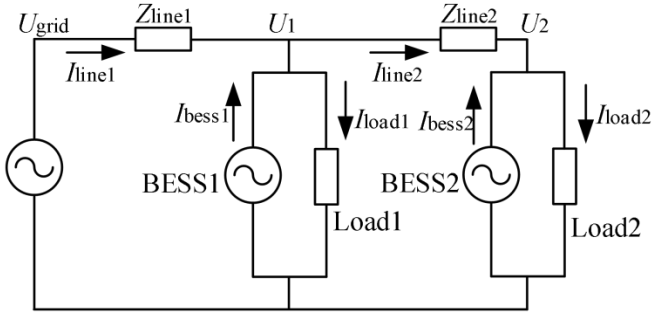

Figure 2. Equivalent circuit of the feeder with integrated distributed energy storage (DES)

In the figure, the current flowing out of the feeder node bus is defined as positive. Based on the direction of the DES current in the circuit, Equation (2) is formulated.

$$\begin{cases} U_1 = U_{\text{ref1}} - k_1 I_{\text{bess1 1 pu}} = U_{\text{grid}} - [(I_{\text{load1}} - I_{\text{bess1 1}}) + (I_{\text{load2}} - I_{\text{bess 2}})]Z_{\text{line1}} \\ U_2 = U_{\text{ref 2}} - k_2 I_{\text{bess2_pu}} = U_{\text{grid}} - [(I_{\text{load1}} - I_{\text{bess1}}) + (I_{\text{load2 2}} - I_{\text{bess 2}})]Z_{\text{line1 1}} - Z_{\text{line2}} (I_{\text{load2}} - I_{\text{bess2}}) \end{cases} \tag{2}$$

In Equation (2), U_1 and U_2 denote the per-unit voltages at Node 1 and Node 2, respectively. U_{ref1} and U_{ref2} are the per-unit voltage references of the controllers for BESS1 and BESS2. I_{load1} and I_{load2} represent the total per-unit currents of loads and generators at Node 1 and Node 2, respectively. U_{grid} is the per-unit value of the rated grid voltage. Z_{Line1} is the per-unit impedance from Node 1 to the substation, and Z_{Line2} is the per-unit impedance between Node 1 and Node 2. I_{BESS1} and I_{BESS2} are the per-unit currents of BESS1 and BESS2.

The per-unit reference for voltage ($U_1, U_2, U_{\text{ref1}}, U_{\text{ref2}}, U_{\text{grid}}$) is the rated voltage, while the per-unit base for currents ($I_{\text{load1}}, I_{\text{load2}}, I_{\text{BESS1}}, I_{\text{BESS2}}$) is the rated feeder current. $I_{\text{BESS1_pu}}$ and $I_{\text{BESS2_pu}}$ denote the per-unit currents of BESS1 and BESS2 using the DES-rated current as the base,

differing from $I_{\text{BESS1}}$and I_{BESS2}. $k_1$and $k_2$are the droop slopes set by the controllers of Node 1 and Node 2, respectively.

By setting the reference voltages of BESS1 and BESS2 controllers equal to the rated grid voltage, i.e., $U_{\text{ref1}} = U_{\text{ref2}} = U_{\text{grid}}$, the ratio of $k_1$to $k_2$can be obtained as shown in Equation (3).

$$\frac{k_2}{k_1} = 1 + \frac{Z_{\text{line 2}}}{Z_{\text{line1 1}}} \cdot \frac{I_{\text{bess1_pu}}}{I_{\text{bess 2 ppu}}} \cdot \frac{I_{\text{load2}} - I_{\text{bess 2}}}{(I_{\text{load 1}} - I_{\text{bess 1}}) + (I_{\text{load 2}} - I_{\text{bess 2}})} \tag{3}$$

When extending to a feeder with Nnodes, the voltage deviation at Node $n-2$from its rated voltage is neglected, i.e., the voltage at Node $n-2$is assumed equal to the rated voltage. Under this assumption, the droop slope $k_n$of the DES at Node $n$and the droop slope $k_{n-1}$of the DES at Node $n-1$satisfy the relationship shown in Equation (4).

$$\frac{k_{\text{n}}}{k_{\text{n}-1}} = 1 + \frac{Z_{\text{line (n)}}}{Z_{\text{line (n}-1)}} \cdot \frac{I_{\text{bess (n}-1)\text{pu}}}{I_{\text{bess (n)}_{\text{pu}}}} \cdot \frac{I_{\text{load (n)}} - I_{\text{bess (n)}}}{(I_{\text{load(n-1)}} - I_{\text{bess (n}-1)}) + (I_{\text{load (n)}} - I_{\text{bess (n)}})} (n = 2 \dots N) \tag{4}$$

In Equation (4), $Z_{\text{line}(n)}$denotes the per-unit impedance of the line connecting Node $n$and Node $n-1$, while $Z_{\text{line}(n-1)}$is the per-unit impedance of the line between Node $n-1$and Node $n-2$(note: Node 0 is the substation connected to the feeder). $I_{\text{BESS}(n)}$and $I_{\text{BESS}(n-1)}$represent the per-unit currents of the BESS units at Node $n$and Node $n-1$, respectively, and $I_{\text{load}(n)}$and $I_{\text{load}(n-1)}$denote the total per-unit load and generator currents at Node $n$and Node $n-1$, respectively. The per-unit base for $I_{\text{load}(n)}$, $I_{\text{load}(n-1)}$, $I_{\text{BESS}(n)}$, and $I_{\text{BESS}(n-1)}$is the rated feeder current. $I_{\text{BESS}(n)_pu}$and $I_{\text{BESS}(n-1)_pu}$are the per-unit currents of BESS at Node $n$and Node $n-1$based on the DES-rated current, and $k_n$and k_{n-1}denote the droop slopes set by the controllers at Node n and Node $n-1$, respectively.

From Equation (4), it can be seen that each droop slope depends on line impedance, load current, and DES current, making the setting procedure highly complex. To simplify the calculation of droop slopes for multiple BESS units, this paper proposes a distributed DES droop coefficient setting method that considers both line impedance and storage capacity.

When the loads at all nodes reach their maximum, the DES at each node also operates at its rated capacity. This ensures that no single DES reaches its limit prematurely while other units still have significant remaining capacity. At the maximum DES output, $I_{\text{BESS}(n-1)_pu_max}$ and $I_{\text{BESS}(n)_pu_max}$are both 1.0 pu, and the droop slopes can be set according to Equation (5).

$$\frac{k_{\text{n}}}{k_{\text{n}-1}} = 1 + \frac{Z_{\text{line (n)}}}{Z_{\text{line (n}-1)}} \cdot \frac{I_{\text{load (n) max}} - I_{\text{bess (n) max}}}{(I_{\text{load (n}-1)_{\text{max}}} - I_{\text{bess (n}-1)\ _\text{max}}) + (I_{\text{load (n) max}} - I_{\text{bess (n) max}})} (n = 2 \dots N) \tag{5}$$

Assume that the ratio between the DES capacity and the maximum load power is the same for

all nodes. When the node load reaches its maximum, the output current of the DES providing voltage compensation also reaches its maximum, and each DES operates at the same power factor as its corresponding node. Let ηdenote the capacity ratio between the DES units at Node $n$and Node $n-1$. The calculation of $\eta$is given in Equation (6).

$$\eta = \frac{I_{\text{bess(n)_max}}}{I_{\text{bess(n-1)_max}}} = \frac{S_{\text{n}}}{S_{\text{n-1}}} (n = 2 \dots N) \tag{6}$$

In Equation (6), $S_n$and S_{n-1}denote the capacities of the BESS units at Node $n$and Node $n-1$, respectively. Substituting Equation (6) into Equation (5) yields Equation (7).

$$\frac{k_{\text{n}}}{k_{\text{n}-1}} = 1 + \frac{Z_{\text{line (n)}}}{Z_{\text{line (n}-1)}} \cdot \frac{\eta}{1+\eta} (n = 2 \dots N) \tag{7}$$

Equation (7) can further be simplified to Equation (8) based on the different line lengths between feeder nodes.

$$\frac{k_{\text{n}}}{k_{\text{n}-1}} = 1 + \frac{L_{\text{linec (n)}}}{L_{\text{line (n}-1)}} \cdot \frac{\eta}{1+\eta} (n = 2 \dots N) \tag{8}$$

In the equation, $L_{\text{line}(n)}$represents the length of the line connecting Node $n$and Node $n-1$, while $L_{\text{line}(n-1)}$denotes the length of the line between Node $n-1$and Node $n-2$. Based on the above droop coefficient setting procedure, the following conclusions can be drawn:

(1) Due to the complexity of the droop coefficient calculation, this paper provides only the principle for setting the slopes. Equation (7) is not fully universal. In practical applications, the DES and maximum load configurations should be analyzed to determine the slopes according to the proposed principle, and further verified through simulation to obtain optimal adjusted slopes that meet the requirements of different projects.

(2) The droop slope of the DES at the first feeder node can be obtained empirically, while the slopes of subsequent nodes are determined based on the ratio relative to the preceding node.

(3) The slopes of DES units at feeder nodes follow a specific pattern: the droop slope is directly proportional to the distance between the node and the substation—the farther the node from the substation, the larger the slope. Conversely, the slope is inversely proportional to the DES capacity—smaller-capacity units require larger slopes.

With this configuration, all DES units respond consistently when the load at a node changes, avoiding compensatory or counteractive behaviors among different DES units.

1.2 Multi-Point Voltage Coordinated Control Strategy for Feeders Based

on Distributed Energy Storage Cluster Control

After introducing the droop slopes, the voltage coordinated control strategy for the DES cluster is illustrated in Fig. 3. Each DES unit adopts the same voltage control strategy. Consider a feeder with Nnodes equipped with DES units. For the n-th DES unit ($n = 1,2,3,\dots,N$), the product of its per-unit output current $I_{\mathrm{BESS}(n)_pu}$ and the regulation droop slope $k_{\mathrm{pu}(n)}$ is used as a negative feedback signal. This is subtracted from the reference voltage $U_{\mathrm{pccrms_ref}}$ to form a new reference voltage for the voltage control loop.

The resulting voltage is then compared with the actual voltage at the DES connection point, $U_{\mathrm{pccrms}(n)}$, and a PI controller generates the reference current $i_{\mathrm{ref}}(n)$ for the BESS unit.

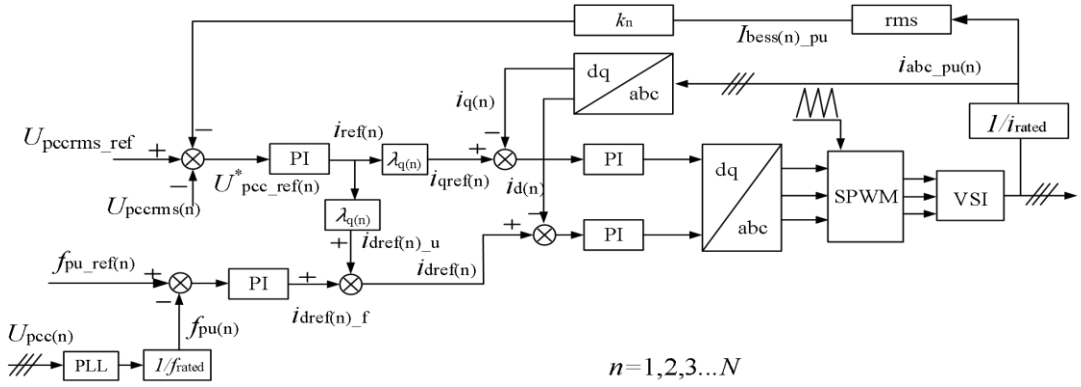

Figure 3. Voltage coordinated control strategy of distributed energy storage (DES)

The current is multiplied by the active power coefficient $\lambda_d(n)$ and reactive power coefficient $\lambda_q(n)$ to generate the active current command $i_{d\mathrm{ref}(n)}$ and reactive current command $i_{q\mathrm{ref}(n)}$, respectively. The active power coefficient $\lambda_d(n)$ corresponds to the power factor of the DES unit. During operation, the power factor can be set either as a fixed value or as load-following at the connection node. A fixed power factor scheme offers a simpler and more reliable control structure but requires careful selection to avoid overcompensation of reactive power. The load-following scheme improves node power regulation accuracy but increases control complexity and requires additional current measurement devices. The choice of scheme should be based on specific engineering conditions.

When a feeder fault results in islanding, the proposed control strategy introduces a frequency regulation loop within the active power control branch to maintain island frequency stability. The actual frequency is obtained via a phase-locked loop (PLL) and compared with the reference value. A PI controller then generates an active current compensation component, which is activated only

when a frequency deviation occurs, achieving stable island frequency control. The DES inverter is controlled in the d–$q$reference frame, with active and reactive currents compared to their respective reference commands to produce voltage references. These voltage references are then transformed and applied to the PWM modulator to drive the inverter, enabling precise coordinated control of active and reactive power for the DES.

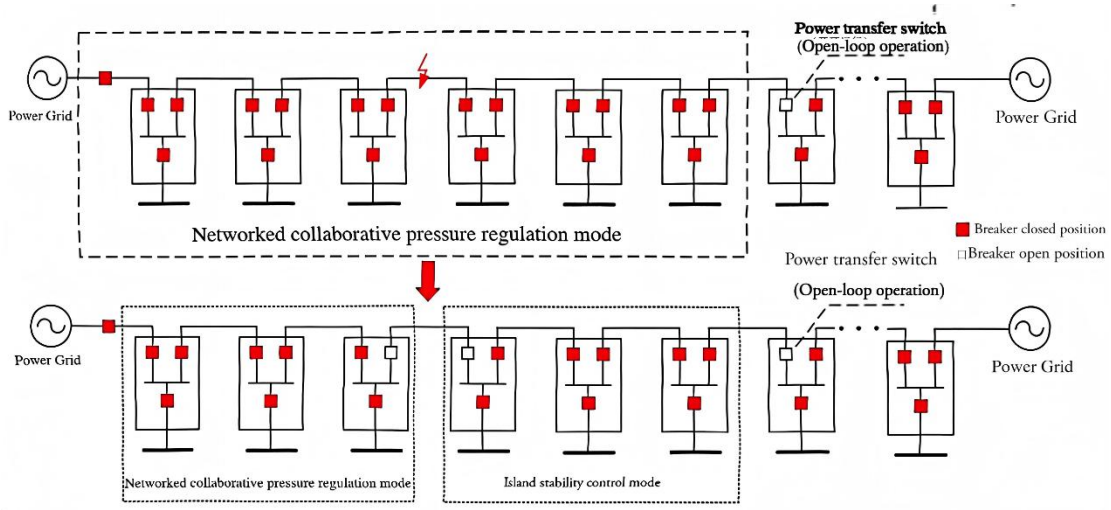

Figure 4. Operating modes of the feeder under grid-connected and islanded conditions

The proposed improved droop control exhibits strong adaptability to changes in distribution network topology and is effective under both grid-connected and islanded modes. In general, the droop slopes do not require real-time updating. Slope adjustments are only necessary when the feeder topology changes due to planned modifications, such as relocating open-loop points or adding T-connections. These changes are predictable, and the droop slopes can be recalculated using the established formulas before each modification. In contrast, unexpected faults or manual operations that alter the topology do not require adjustments to the droop slopes. For example, when a feeder section is isolated due to a fault, the feeder topology changes, forming a grid-connected segment and an islanded segment, as shown in Fig. 4. The DES voltage coordinated control strategy is effective in regulating node voltages in both the grid-connected and islanded areas.

2. Feeder Fault Fast Self-Healing Control Method Based on Distributed Energy Storage Cluster Control

After a feeder fault forms an island, the DES units need to collaboratively regulate the islanded voltage and frequency. Voltage control, as described previously, is effective under both grid-

connected and islanded conditions. However, the frequency control loop must respond according to the feeder operating condition: it should be deactivated during grid-connected operation and activated during islanding. If frequency control is engaged during grid-connected operation, DES units may quickly reach their operating limits. Conversely, if the frequency control loop is not promptly activated during islanding, the islanded network may become unstable. In addition, the state-of-charge (SOC) management of the DES system is critical to ensuring the successful execution of voltage regulation and self-healing functions.

2.1 Frequency Deviation Control Strategy Based on Dual-Hysteresis Comparison

For islanded self-healing, DES units must accurately activate the frequency control loop. The activation must meet the following requirements:

(1) The frequency control loop should be activated promptly and accurately when the feeder forms an island, regulating the island frequency to maintain minimal deviation.

(2) The loop must be robust against frequency fluctuations caused by power disturbances, preventing DES units from entering extreme operating states.

(3) The frequency control loop must deactivate when the island reconnects to the main grid.

To satisfy these requirements, a frequency deviation control method based on a dual-hysteresis comparison strategy is designed, as illustrated in Fig. 5.

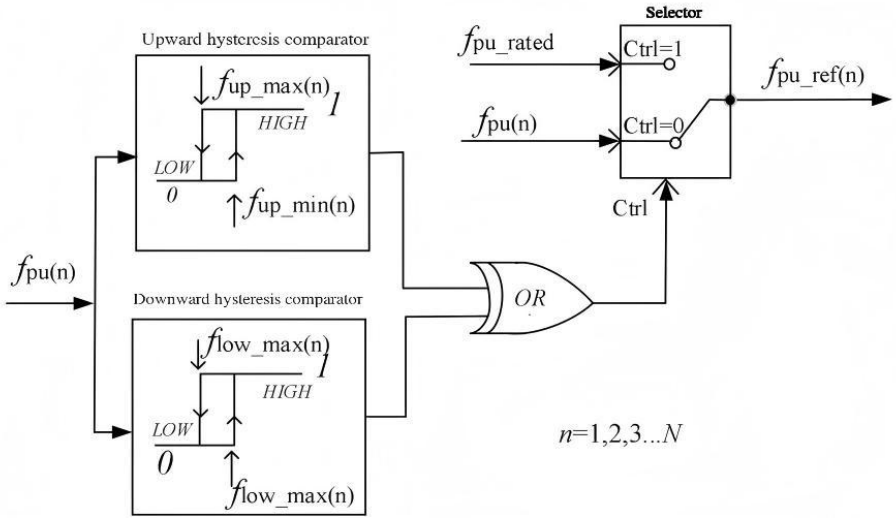

Figure 5. Frequency deviation control strategy based on the dual-hysteresis comparison method

In Fig. 5, $f_{pu}(n)$ denotes the per-unit value of the actual frequency sampled at Node n. During

normal grid-connected operation, the feeder frequency $f_{pu}(n)$ remains within the interval $[f_{low_max}, f_{up_min}]$. In this range, the outputs of both hysteresis comparators are 0, and the selector input $Ctrl = 0$. As a result, the reference frequency $f_{pu_ref}(n)$equals the actual frequency $f_{pu}(n)$, the DES frequency control loop output is zero, and the frequency control target follows the system frequency, effectively deactivating the frequency control loop.

When the feeder is islanded due to a fault, the DES units and local loads form an islanded section, causing the feeder frequency $f_{pu}(n)$to deviate. If $f_{pu}(n) > f_{up_max}$or $f_{pu}(n) < f_{low_min}$, the upward or downward hysteresis comparator output becomes 1, and the selector input $Ctrl = 1$. In this case, the frequency deviation control strategy uses the system nominal frequency f_{pu_base}as the input to the frequency control loop ($f_{pu_ref}(n) = f_{pu_base}$), activating the loop. The DES units then regulate the islanded frequency, restoring it to the nominal value. After the islanded feeder is reconnected to the main grid via reclosing or automatic transfer switching, $f_{pu}(n)$returns to the $[f_{low_max}, f_{up_min}]$interval, the selector sets $Ctrl = 0$, and the DES frequency control target again follows the system frequency, effectively freezing the frequency control loop.

By introducing dual-hysteresis comparators in the frequency control loop, upward and downward frequency deviations are detected, and the DES frequency control loop is activated or frozen according to defined thresholds. This approach gives the frequency control characteristic curve a hysteresis behavior, providing strong immunity to frequency deviations caused by power fluctuations under grid-connected conditions. Consequently, each DES unit can identify feeder islanding accurately and timely without relying on communication, ensuring stable control of islanded feeder frequency.

The frequency deviation control strategy based on dual-hysteresis comparator enablement can also accommodate detection errors caused by power fluctuations. In practical applications, the hysteresis bands can be widened as needed to improve the reliability of island detection.

The proposed distributed energy storage cluster control method covers the entire feeder process from grid-connected operation to islanding and eventual reconnection. The DES control modes under different operating conditions are illustrated in Fig. 6. This method collects voltage and frequency at the common PCC of each node and regulates local voltage and frequency, without requiring information exchange between nodes. Specifically:

(1) Grid-connected operation: DES units operate in voltage coordination mode, controlling

node voltages according to droop slopes.

(2) Fault occurrence: Node voltages drop, and DES units may become uncontrolled, with output currents potentially limited.

(3) Islanded operation: Frequency deviation control is activated to regulate island frequency, while voltage coordination remains effective to maintain island voltages.

(4) Grid restoration: The frequency deviation control loop is frozen, and the coordinated voltage control strategy continues to regulate voltages at all PCC nodes.

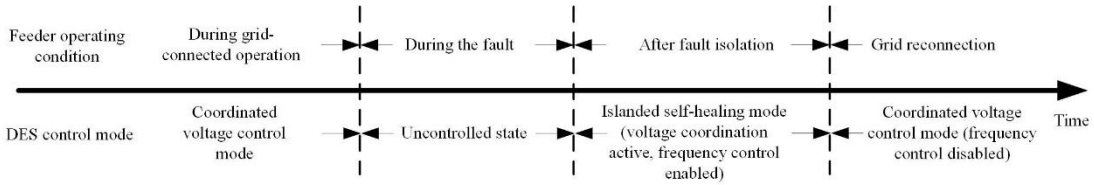

Figure 6. Control modes of distributed energy storage (DES) under different feeder operating conditions

2.2 Optimal SOC Control for Self-Healing Function

During the operation of distributed energy storage (DES), the state of charge (SOC) should be maintained at an optimal level to ensure that the DES can flexibly respond to various scenarios such as voltage regulation and self-healing. During grid-connected operation, each DES unit must retain sufficient capacity to cope with voltage fluctuations caused by feeder power variations. In the event of a feeder fault, adequate SOC reserve ensures stable operation of the islanded feeder. To achieve this, an optimal SOC control method for DES targeting self-healing functionality is proposed. Four SOC operating points are defined: the maximum SOC (SOC_{max}), the upper and lower bounds of the optimal SOC (SOC_{b_max} and SOC_{b_min}), and the minimum SOC (SOC_{min}), as illustrated in Fig. 7.



Figure 7. SOC operating points of distributed energy storage (DES)

The optimal SOC control method for distributed energy storage (DES) is illustrated in Fig. 8. The procedure begins by detecting the current SOC of the DES and determining which SOC range it falls into:

(1) Optimal SOC Range ($SOC_{b_min} \leq SOC \leq SOC_{b_max}$):When the SOC is within the optimal

range, the DES continues to operate in the coordinated voltage control mode, with no adjustments required.

(2) Limit SOC Range ($SOC \geq SOC_{max}$ or $SOC \leq SOC_{min}$):When the SOC reaches or exceeds the operational limits, the DES exits the coordinated voltage control mode and is forced into a trickle charge/discharge mode until the SOC is brought back into the optimal range$[SOC_{b_min}, SOC_{b_max}]$.

(3) Intermediate SOC Range ($SOC_{min} < SOC < SOC_{b_min}$ or $SOC_{b_max} < SOC < SOC_{max}$):In this range, the participation of DES in coordinated voltage control depends on the minimum current threshold I_{set_min}:

If $I_{BESS} \leq I_{set_min}$, the node voltage is considered sufficient, and the DES can enter trickle charge mode until the SOC returns to $[SOC_{b_min}, SOC_{b_max}]$.

If $I_{BESS} > I_{set_min}$, the SOC control must consider the current operating state:

For $SOC_{b_max} < SOC < SOC_{max}$ during charging, the SOC may exceed SOC_{max}; the DES is switched to trickle discharge until it returns to the optimal range. If discharging, the current operation continues unchanged.

For $SOC_{min} < SOC < SOC_{b_min}$ during discharging, continued operation may drive SOC below SOC_{min}; the DES is switched to trickle charge until the SOC returns to $[SOC_{b_min}, SOC_{b_max}]$. If charging, the current operation continues unchanged.

This strategy ensures that each DES maintains sufficient flexibility to support voltage regulation and feeder self-healing while keeping SOC within safe and optimal limits.

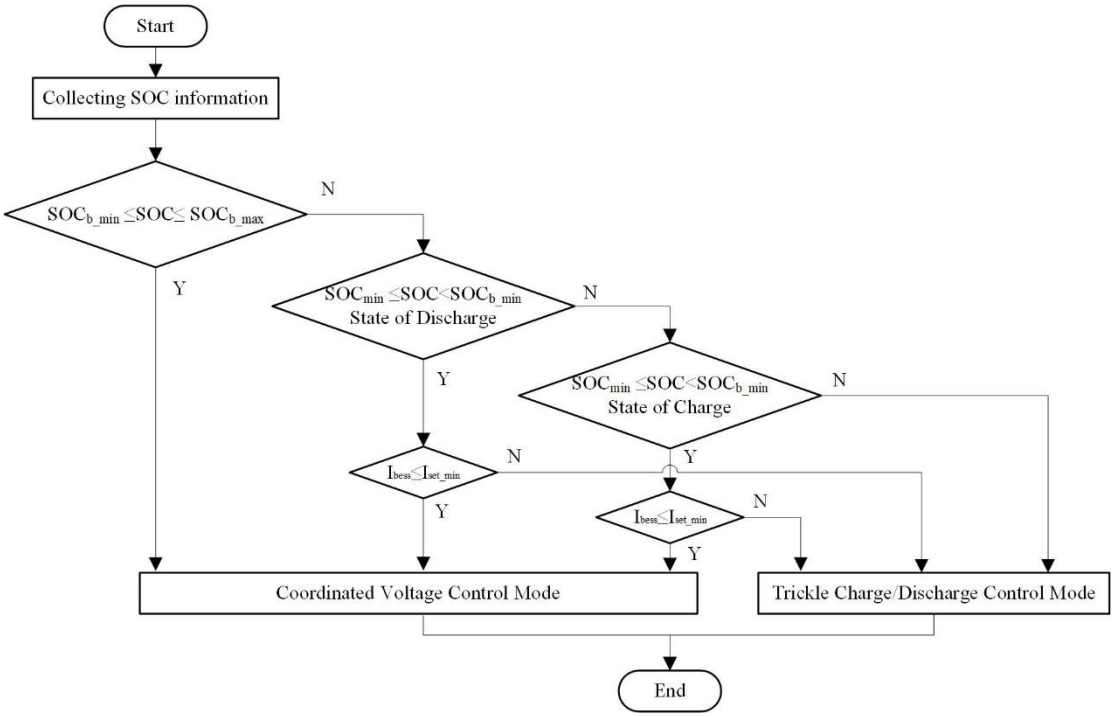

Figure 8. Optimal SOC Control Method of Distributed Energy Storage Oriented to Fault Self-Healing Function

Through the above control strategy, the energy storage system can be ensured to maintain a favorable state of charge (SOC) at any time, thereby providing adequate preparation for feeder islanding self-healing. Continuous charging or continuous discharging is the most unfavorable condition for SOC control. Under these two operating modes, the SOC may transition from SOC_{b_min} to SOC_{min} or from SOC_{b_max} to SOC_{max}. Therefore, it is necessary to impose constraints on the charging and discharging control cycles of the energy storage system, as defined in Equations (9) and (10).

$$T_1 = \frac{SOC_{\mathrm{b_min}} - SOC_{\mathrm{min}}}{P_{\mathrm{char_max}}} \tag{9}$$

$$T_2 = \frac{SOC_{\mathrm{b_min}} - SOC_{\mathrm{min}}}{P_{\mathrm{disc_max}}} \tag{10}$$

In Equations (9) and (10), P_{char_max} represents the maximum charging power of the energy storage system, and P_{disc_max} represents the maximum discharging power. T_1 is the minimum time required for the SOC to decrease from SOC_{b_min} to SOC_{min} during discharging, and T_2 is the minimum time required for the SOC to increase from SOC_{b_max} to SOC_{max} during charging.

To prevent the SOC from exceeding SOC_{max} due to continuous charging or dropping below SOC_{min} due to continuous discharging, the charging/discharging control period T should be set to

the smaller value of $T_1$and T_2, as shown in Equation (11). In addition, it should be noted that the duration of trickle charging and discharging control is not included in the control period.

$$T = min[T_1, T_2] \tag{11}$$

3 Real-Time Simulation Verification

To verify the effectiveness of the distributed energy storage (DES) coordinated voltage regulation and fault self-healing functions, this paper establishes detailed models of the DES primary system and control strategies, and constructs a real-time closed-loop simulation system integrating RTDS and actual line protection devices. Simulations are carried out for feeder-connected coordinated voltage control and rapid feeder fault self-healing, and the results demonstrate the correctness of the proposed methods.

3.1 Simulation Platform Setup

The real-time simulation platform is shown in Fig. 9. A 10 kV feeder model with three power supply nodes is built in the RTDS real-time simulator. At each node, all loads and distributed generation units are equivalently aggregated into a single load and a single generation unit, respectively. Together with the distributed energy storage, they are connected to the 10 kV feeder through a common transformer. The three nodes are interconnected via overhead lines of type LGJ-95, and then connected to the main grid through a 10/110 kV transformer.

Circuit breakers are installed at both ends of each feeder section between nodes, namely BRK1, BRK2, BRK3, BRK4, BRK5, and BRK6. Each circuit breaker is equipped with line differential protection, with protection settings configured according to system parameters. The PT and CT signals simulated by RTDS are output through the GTAO interface cards and then, via voltage and current power amplifiers, are fed into the line protection devices. Meanwhile, the circuit breaker status signals are transmitted to the protection devices through the GTDO interface cards. When a fault occurs in the system, the protection devices issue trip commands, which are fed back to RTDS through the GTDI interface cards, thereby forming a complete closed-loop simulation system. Interphase faults are set at locations K2, K3, and K4 on lines line1, line2, and line3, respectively.

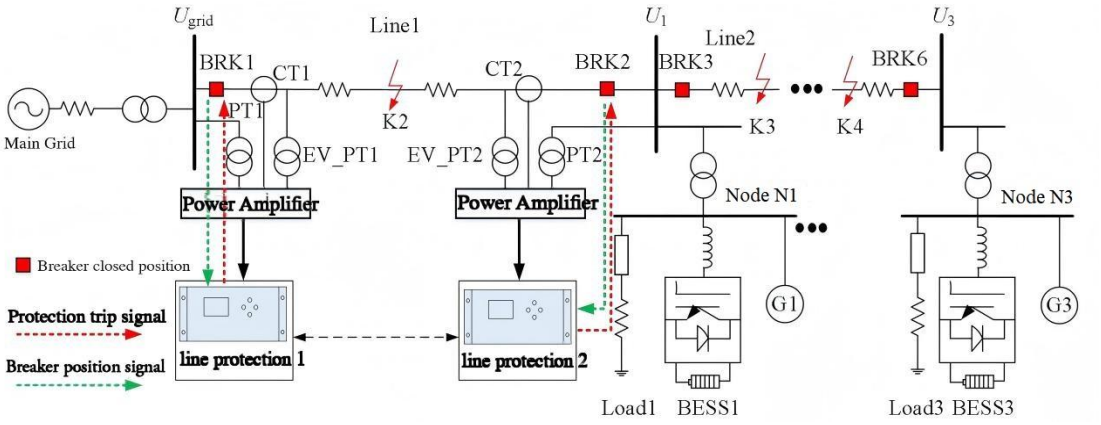

Figure 9. Real-Time Closed-Loop Simulation System for Distributed Energy Storage Cluster Control

The main parameters of the energy storage model are shown in Table 1.

Table 1 Main Parameters of the Energy Storage Model

Component	Parameter	Value		
Distributed Energy Storage System (DESS)	BESS1	Capacity:	1MVA	Droop Coefficient:0.03
	BESS2	Capacity:	1.2MVA	Droop Coefficient:0.04
	BESS3	Capacity:	1.4MVA	Droop Coefficient:0.05

The main parameters of the Feeder model are shown in Table 2.

Table 2 Main Parameters of the Feeder Model

Component	Parameter	Value		
Main Grid	Voltage Level, Short-Circuit Capacity	110kV、300MW		
Transformer	Connection Type, Turns Ratio, Capacity	110/10kV、Y/D11 48MW		
Line	Positive-Sequence Impedance, Zero-Sequence Impedance	0.3302/km、0.3902/km		
	Length	Linel	Line2	Line3
		5km	4km	3km
PTg、Voltage、Current Sensors	PT1、PT2、PT3、 PT EV1、 PT EV2、PT EV3	10kV/0.1kV		
	CT1、CT2	600A/1A		
	CT3、CT4	450A/1A		
	CT5、CT6	300A/1A		

In the simulation, depending on the operating period, the load is classified into heavy-load and light-load modes, as shown in Table 3.

Table 3 Feeder Load Simulation Parameters under Light and Heavy Load Conditions

Object	Heavy Load		Light Load	
	Active Power	Reactive Power	Active Power	Reactive Power
L Load 1	1.2MW	0.6MVar	0.24M W	0.12M Var

L Load2	1.4MW	0.7MVar	0.28M W	0.14M Var
L oad3	1.6MW	0.8MVar	0.32MW	0.16M Var

In the simulation, the output of small hydropower plants under high-flow and low-flow conditions is shown in Table 4.

Table 4 Small Hydropower Output Parameters under High-Flow and Low-Flow Conditions

Object	High-Flow Period		Low-Flow Period	
	Active Power	Reactive Power	Active Power	Reactive Power
Gen1	-1.1MW	-0.33M Var	-0.33MW	-0.1MVar
Gen2	-1.3MW	-0.39M Var	-0.39MW	-0.11MVar
Gen3	-1.5M W	-0.45MVar	-0.45MW	-0.13M Var

The 10 kV Feeder Protection Settings is shown in Table 5.

Table 5 10 kV Feeder Protection Settings

Category	Setting Name	Setting Item	Protection Configured for BRK1, BRK3, BRK5	Protection Configured for BRK2, BRK4, BRK6
Setting Name	Longitudinal Differential Protection	Differential Operation Current Setting	0.8A	0.8A
	Reclosing	Reclosing Synchronism Angle, Voltage, Frequency Setting	\	±30°、±15.0V、±0.5Hz

Due to the large number of simulation scenarios, the meanings of the various curve labels in the simulation figures are listed in Table 6.

Table 6 Meanings of Curves in Feeder Fault Self-Healing Simulation Results

Name	Description
Ugrms 、 U1rms 、 U2rms 、U3rms U1rmsref 、 U2rmsref 、U3rmsref	Ugrms, U1rms, U2rms, U3rms – Per-unit RMS voltages at the central substation and nodes 1, 2, and 3, respectively. U1rmsref, U2rmsref, U3rmsref – Per-unit reference voltages of BESS1, BESS2, and BESS3, respectively.
fpu_area1 、 fpu_area2、 fpu_area3fpu_ref1 、 fpu_ref2、 fpu_ref3	fpu_area1, fpu_area2, fpu_area3 – Per-unit frequencies of Areas 1, 2, and 3, respectively. fpu_ref1, fpu_ref2, fpu_ref3 – Frequency control reference values of BESS1, BESS2, and BESS3, respectively.
Pload1 、 Qload1 、Pload2、Qload2,Pload3 、 Qload3	The active and reactive power of the load at Node 1, Node 2, and Node 3, respectively.

PGen1 、QGen1、PGen2 、QGen2、PGen3 、QGen3	The active and reactive power of the small hydropower units at Node 1, Node 2, and Node 3, respectively.
Pbess1 , Qbess1、Pbess2 , Qbess2、Pbess3 , Qbess3	The active and reactive power of the energy storage systems BESS1 at Node 1, BESS2 at Node 2, and BESS3 at Node 3, respectively.
PLine1 、QLine1 、PLine2 、QLine2PLine3 、QLine3	The active and reactive power of Feeder 1, Feeder 2, and Feeder 3, respectively.
UgA_sec 、UgB_sec 、UgC_sec	The secondary-side voltage of the substation bus PT.
U1A_sec 、U1B_sec 、U1C_sec	The secondary-side voltage at Node 1.
IBRK1A_sec 、IBRK1A_sec 、IBRK1A_sec	The secondary current of the BRK1 circuit breaker CT.
IBRK2A_sec 、IBRK2A_sec 、IBRK2A_sec	The secondary current of the BRK2 circuit breaker.
BRK1_Sta、BRK2_StaBRK3_Sta、BRK4_Sta	The position status of circuit breakers BRK1, BRK2, BRK3, BRK4, BRK5, and BRK6.
BRK1_Trip、BRK2_Trip、BRK3_Trip、BRK4_Trip、BRK5_Trip、BRK6_Trip	The trip commands sent by each protection device to circuit breakers BRK1, BRK2, BRK3, BRK4, BRK5, and BRK6.
BRK1_RCL1、BRK1_RCL2、BRK1_RCL3、BRK1_RCL4、BRK1_RCL5、BRK1_RCL6、	The reclosing commands sent by each protection device to circuit breakers BRK1, BRK2, BRK3, BRK4, BRK5, and BRK6.
Fault_K4	Fault trigger commands for K2, K3, and K4.

3.2 Simulation Validation

To verify the effectiveness of the proposed method, two scenarios are simulated on the real-time simulation platform: the distributed energy storage (DES) coordinated voltage control under the grid-connected feeder scenario, and the DES fault self-healing under the islanded feeder scenario. For consistency, all loads, small hydropower units, and DES power directions are defined as positive when flowing out of the bus (load consumption), and negative when flowing into the bus (generation output).

Scenario 1: Grid-connected feeder – DES coordinated voltage control simulation

Under grid-connected operation, the outputs of the loads or generation units at the three nodes are varied to compare the cases with and without DES participation, demonstrating the effect of DES coordinated voltage control. Since small hydropower outputs remain relatively stable over long periods, while node loads fluctuate randomly, this simulation models alternating load variations at the three nodes under both high-flow and low-flow conditions.

1) Case1: High-flow season, DES group inactive

During the high-flow period, small hydropower output reaches its maximum. DES units are inactive, and load power fluctuations are simulated to represent both high-flow large and high-flow small scenarios. Trends of node voltages, load power, small hydropower output, and line power are shown in Fig. 10.

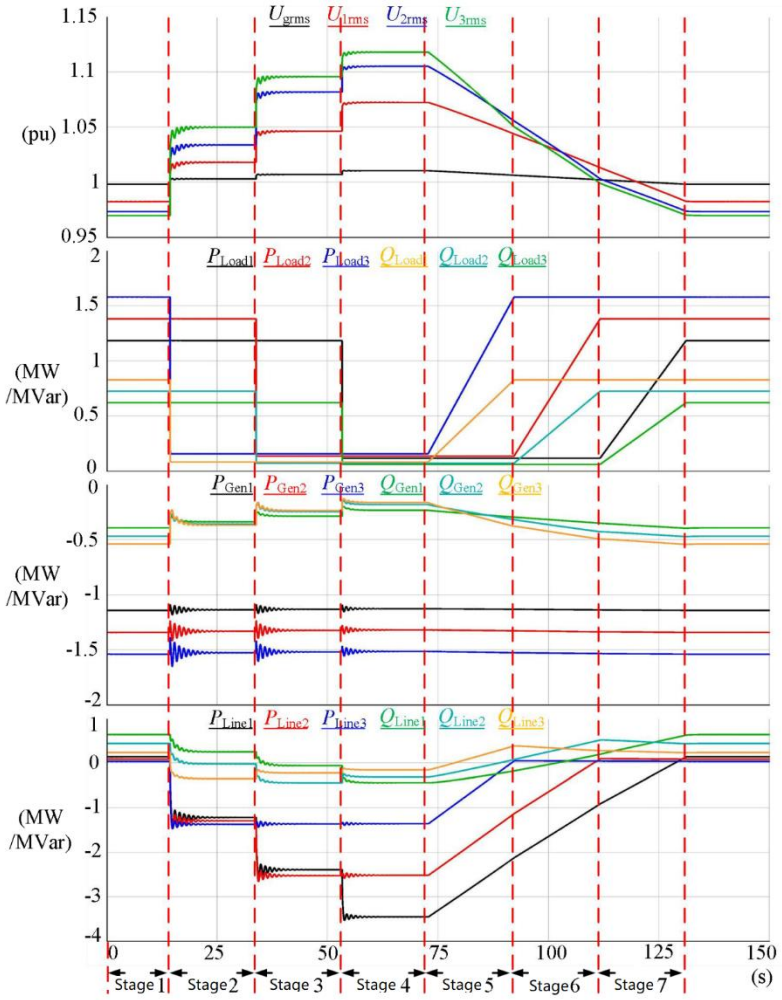

Figure 10. Voltage and power variation trends at each feeder node during the high-flow season with distributed energy storage not in operation.

The simulation is divided into seven stages.

In Stage 1, during the high-flow season under heavy load, small hydropower output nearly balances the load, resulting in limited power exchange with the grid and small voltage deviations. The feeder operates in a high-generation–high-load mode.

In Stages 2–4, the loads at Nodes 3, 2, and 1 successively step from heavy to light. Distributed generation exceeds load demand, causing power to be exported to the grid and node voltages to rise

continuously. In Stage 4, the feeder operates in a high-generation–low-load mode, and node voltages exceed the allowable limits, indicating a serious overvoltage risk.

In Stages 5–7, the loads at Nodes 3, 2, and 1 gradually return from light to heavy. Feeder power transfer decreases and node voltages progressively recover to normal levels. Overall, node voltages increase with feeder power transfer, while small hydropower active power remains constant and its reactive power slightly decreases as voltage rises.

2) Case 2: High-flow season with the distributed energy storage (DES) group in operation.

When the distributed energy storage (DES) group is in service, load variations are identical to the previous case. During load step changes, BESS units simultaneously absorb active and reactive power, effectively suppressing voltage deviations at each node. During gradual load changes, power variations are jointly shared by all BESS units. Throughout the simulation, node voltages are maintained within 0.99–1.04 pu and distributed proportionally with distance from the substation. Active and reactive power are evenly allocated among the BESS units, achieving coordinated control and significantly improving voltage profiles under severe load fluctuations.

Minor oscillations in the BESS reference voltage appear only during power direction reversals, with an amplitude below 0.004 pu, and have negligible impact on overall control performance, as illustrated in Fig. 11.

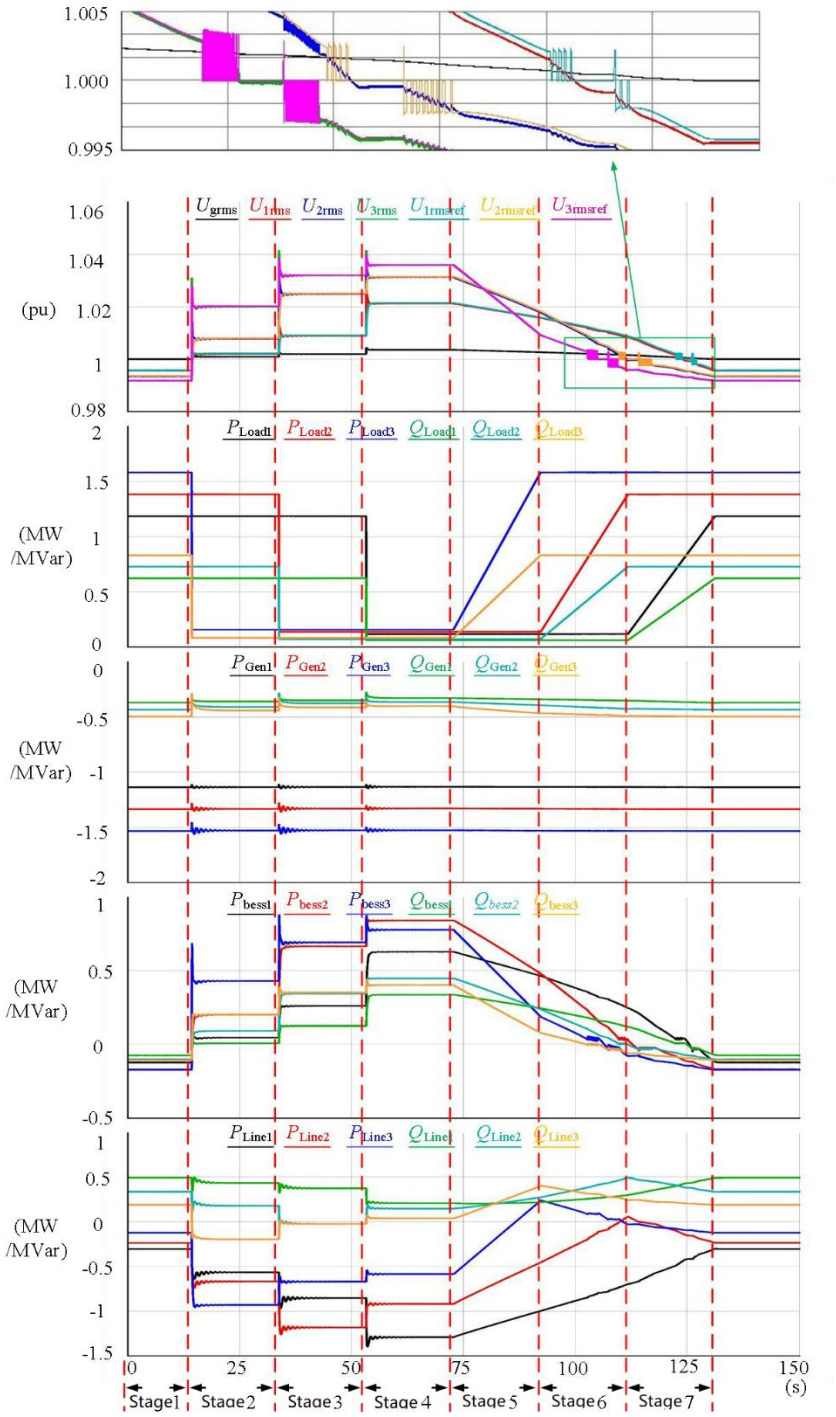

Figure 11. Voltage and power profiles of feeder nodes during the high-flow season with distributed energy storage in service

3) Case 3: Dry season with the distributed energy storage group not in service

During the dry season, the distributed energy storage (DES) group is not put into operation, and variations in load power are simulated. The voltage profiles of feeder nodes, load power variations, small hydropower output, and feeder power flow are shown in Fig. 12.

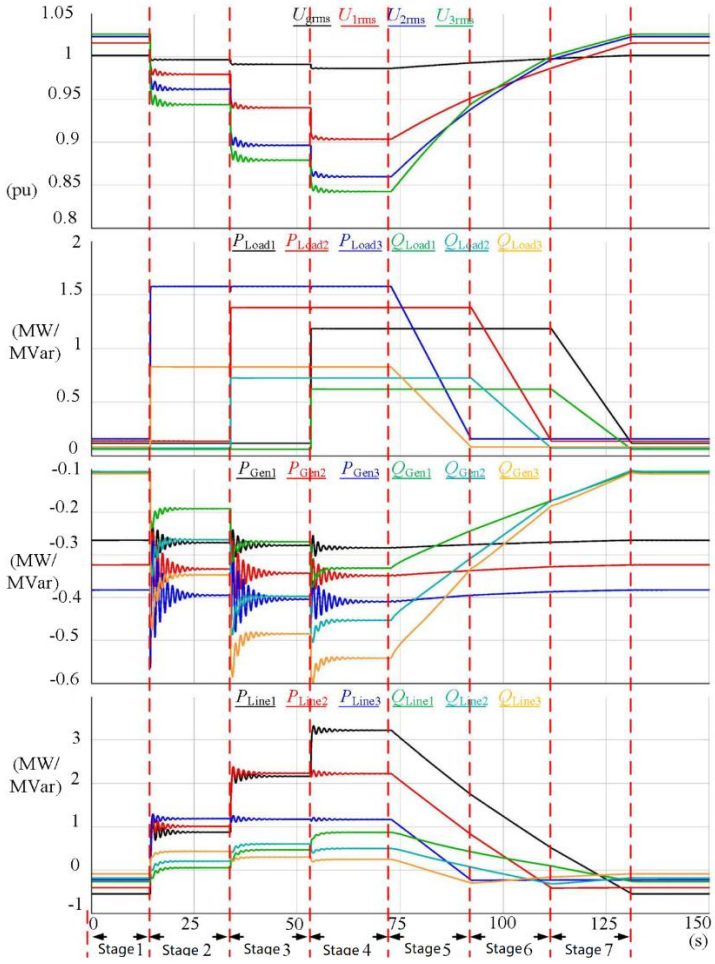

Figure 12. Voltage and power profiles of feeder nodes during the dry season without distributed energy storage in service

From the seven simulation stages, the following observations can be made.

In 1, during the dry season with minimum small hydropower output and light load conditions, generation and load are approximately balanced, resulting in small voltage deviations at all nodes.

In Stage 2, the load at Node 3 steps from light to heavy, causing voltages at all nodes to decrease. In Stage 3, the load at Node 2 steps from light to heavy, further reducing node voltages; the voltages at Nodes 2 and 3 drop below 0.9 pu, violating the lower voltage limit.

In Stage 4, the load at Node 1 steps from light to heavy, leading to the lowest voltage levels along the feeder. The voltage at Node 3 drops to approximately 0.87 pu and at Node 4 to about 0.85 pu. Stage At this point, the feeder operates in a low-generation–high-load mode, and voltage deviations exceed national standard limits.

In Stages 5–7, the loads at Nodes 3, 2, and 1 gradually decrease from heavy to light. As the load is reduced, feeder power transfer decreases and node voltages progressively recover to normal

levels. Overall, under the low-generation–high-load operating mode, the feeder is prone to undervoltage violations.

4) Case 4: Dry season with the distributed energy storage group in service

During the dry season, the distributed energy storage (DES) group is put into operation and load power variations are simulated. The voltage profiles of feeder nodes, load power variations, small hydropower output, and feeder power flow are shown in Fig. 13.

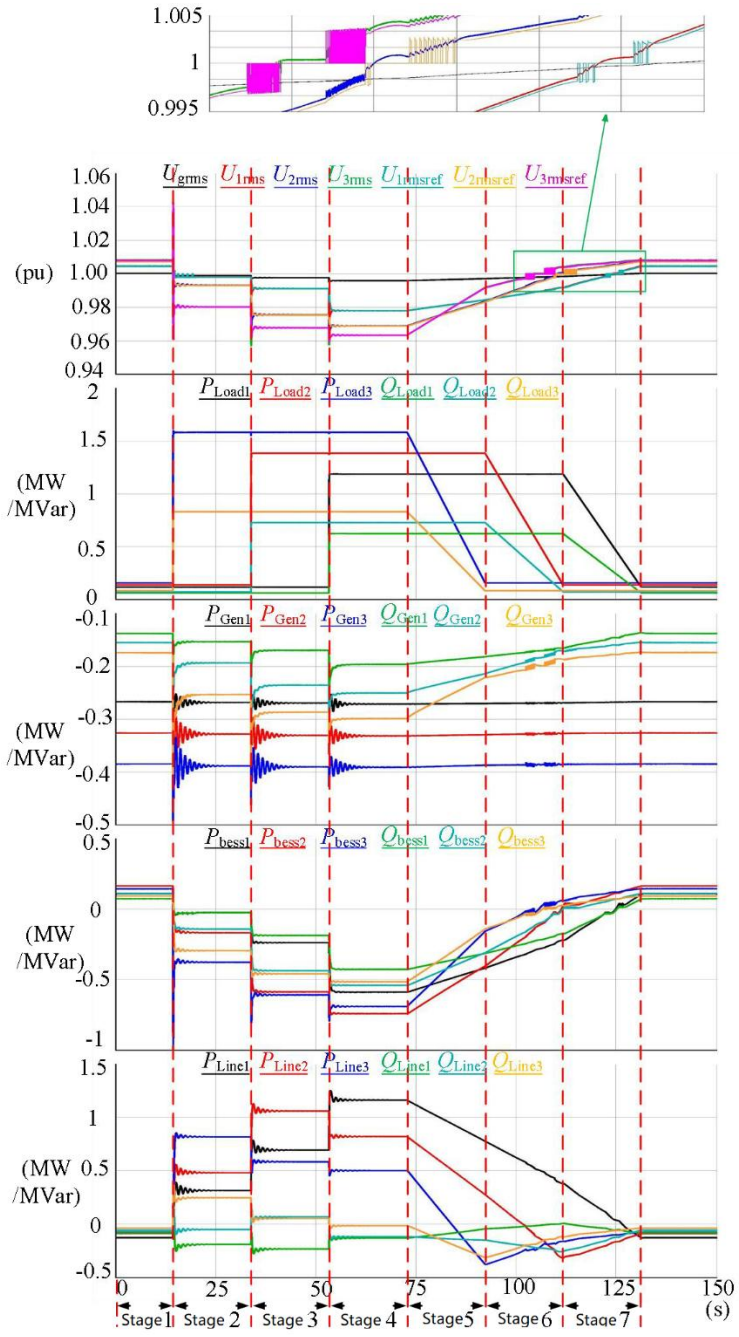

Figure 13. Voltage and power profiles of feeder nodes during the dry season with distributed energy

storage in service

He load power fluctuations at each node are consistent with Case 3, and small hydropower output is relatively low during the dry season. From the seven simulation stages:

Stage 1 to Stage 2: As the load at Node 3 steps from light to heavy, the active and reactive power output of BESS1, BESS2, and BESS3 simultaneously increase, suppressing voltage deviations caused by the load step.

Stage 2 to Stage 3: When Node 2's load steps from light to heavy, the DES cluster absorbs both active and reactive power instantaneously, mitigating voltage deviations at Node 2.

Stage 3 to Stage 4: Similarly, the DES cluster instantly absorbs the load step at Node 1.

Stages 5 to 7: Gradual load changes at all nodes are shared collectively by BESS1, BESS2, and BESS3.

Throughout the simulation, the voltages at Nodes 2 and 3 are maintained between 0.97–1.01 pu and decrease proportionally with distance from the central substation. Step or gradual load changes at any node are distributed among BESS1, BESS2, and BESS3, with active and reactive power shared evenly, achieving coordinated control. Under severe load fluctuations, the feeder node voltage profile is significantly improved, demonstrating the effectiveness of the proposed voltage coordination strategy. Minor oscillations in the reference voltage, as shown in the magnified portions of Figure 13, have been previously explained and are not repeated here.

Scenario 2: Fast Self-Healing Simulation of DES During Feeder Faults

During wet-season light-load or dry-season heavy-load conditions, faults are simulated at midpoints of Line1, Line2, and Line3 (K2, K3, K4). After line protection trips the circuit breakers, the DES units regulate the islanded feeder in Area 1, Area 2, or Area 3. The areas are illustrated in Figure 14. Subsequently, the feeder protection recloses, restoring grid connection and achieving fast self-healing.

To provide a clear comparison, four cases are considered:

Case 1: Wet-season, heavy-load, ABCN fault at K2 forming an island in Area 1.

Case 2: Wet-season, light-load, ABCN fault at K2 forming an island in Area 1.

Case 3: Dry-season, heavy-load, BC fault at K3 forming an island in Area 2.

Case 4: Wet-season, light-load, ABN fault at K4 forming an island in Area 3.

Case 1 easily satisfies reclosing conditions, while Cases 2, 3, and 4 require DES self-healing

control to meet reclosing criteria. To compare extreme conditions, DES is not activated in Case 1, but is enabled in Cases 2, 3, and 4.

1) Case 1: DES Not Activated, High-Generation Mode, ABCN Fault at K2

In high-generation mode without DES, an ABCN fault occurs at K2. Before the fault, Line1 power is -0.22 MW active and -0.08 MVar reactive (exported from Area 1 to the substation). After the fault, the feeder forms an island. The voltage trends at feeder nodes, load power, small hydropower output, line power, BRK1/BRK2 switch states, and trip/reclosing commands are shown in Figure 14.

At T1, an ABCN fault occurs at K2 on Line1, lasting 100 ms. Differential protection at BRK1 and BRK2 operates. After 83 ms, at T2, BRK1 and BRK2 trip, forming an island in Area 1, and feeder voltage and frequency begin to rise.

After approximately 1000 ms (reclosing setting time), at T3, Protection 1 recloses. Protection 2 compares line and node voltages. Reclosing proceeds only if synchronization conditions are satisfied. At this point, due to significant voltage and frequency deviations in the Area 1 island, synchronization fails, and reclosing is unsuccessful—the island cannot reconnect to the grid.

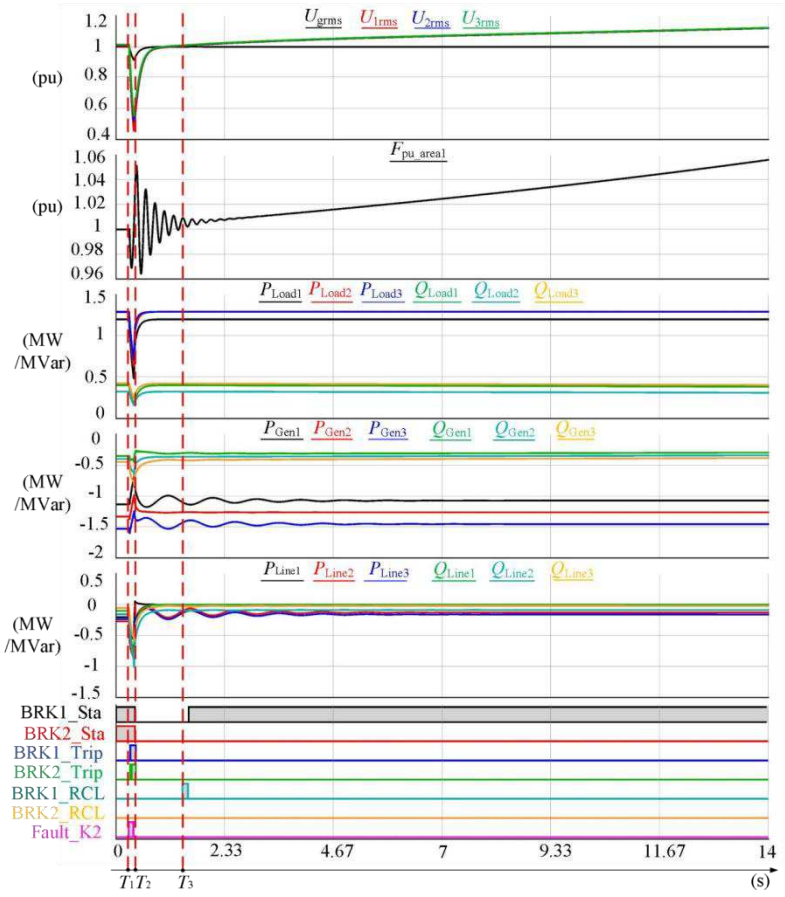

Figure 14. Voltage and Power Trends at Each Node of the Feeder K2 Fault in High-Generation Mode with Distributed Energy Storage Not Activated

Case 2: Distributed Energy Storage Activated, Low-Load–High-Generation Mode, ABCN Fault at K2

In the low-load–high-generation mode, the distributed energy storage (DES) group is activated. An ABCN fault occurs at point K2. Before the fault, Line 1 transfers active power of -1.63 MW (exported to the substation) and reactive power of 0.56 MVar (imported from the substation), i.e., the feeder in Area 1 exports 1.63 MW active power to the substation and absorbs 0.56 MVar reactive power.

As shown in Figure 15, at time T1, the ABCN fault occurs at K2, lasting 100 ms. Differential protection installed at BRK1 (Protection 1) and BRK2 (Protection 2) operates. After 88 ms, at T2, BRK1 and BRK2 trip, forming an isolated feeder (island) in Area 1. At the initial moment of islanding, due to power imbalance, the island voltage rises to 1.03 pu. The DES voltage coordination control strategy quickly regulates the voltage back to its rated value, while the frequency deviation control strategy is activated to bring the island frequency to its rated value.

After the reclosing delay, at T3, Protection 1 recloses successfully, and Protection 2 starts the synchronization check. At T4, Protection 2 recloses successfully, restoring Area 1 to grid connection. The total duration from fault occurrence to island reconnection is approximately 3207 ms. After reconnection, the DES group resumes coordinated voltage control mode.

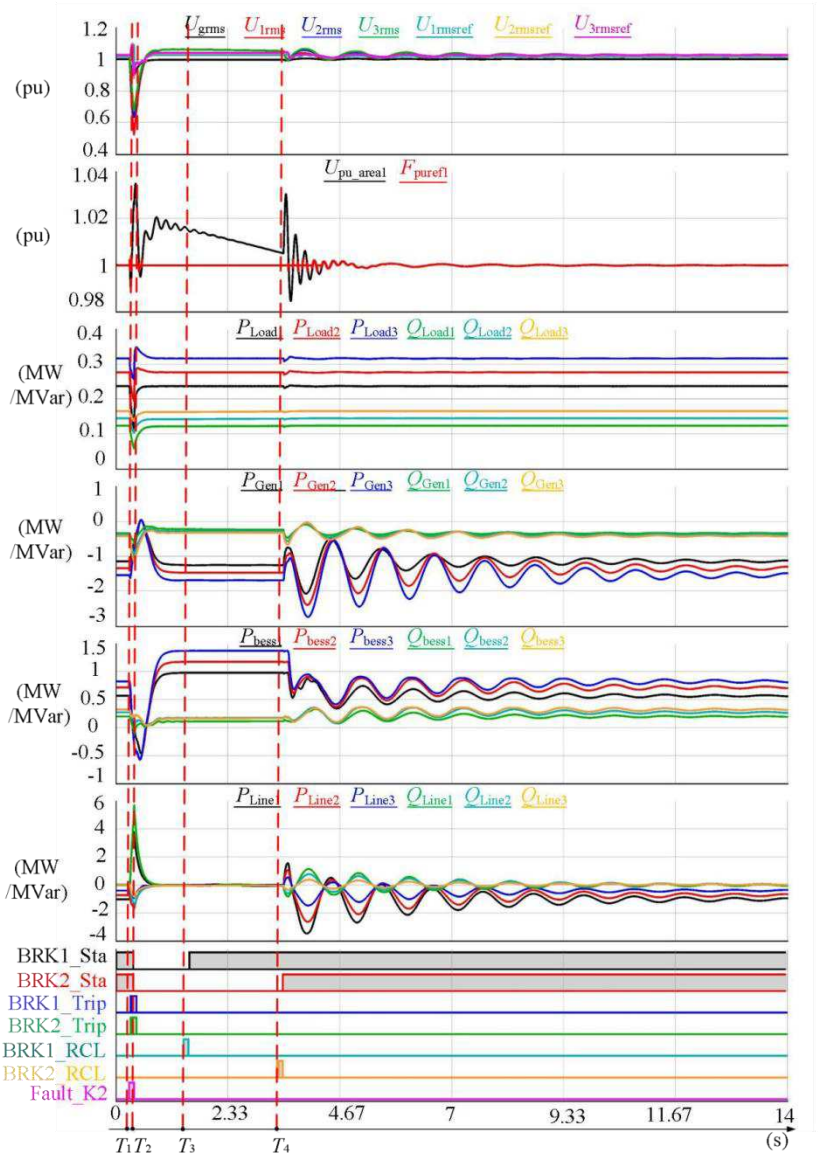

Figure 15. Voltage and Power Trends at Each Node for Feeder K2 Fault in High-Generation–Low-Load Mode with Distributed Energy Storage Activated

The secondary voltages and currents at Protection 1, and the secondary voltage, extracted voltage, and current at Protection 2, are shown in Figure 16. At T1, a fault occurs at K2 on the feeder, causing a voltage drop at the substation. Both Protection 1 and Protection 2 detect an increase in fault current, triggering the line differential protection. At T2, the breakers on both ends of Line 1 trip. By T3, Protection 1 recloses, closing BRK1, while Protection 2 monitors the line's extracted voltage and initiates the synchrocheck assessment. At T4, Protection 2 confirms that the synchrocheck conditions are satisfied, successfully recloses BRK2, and the feeder is restored to grid connection.

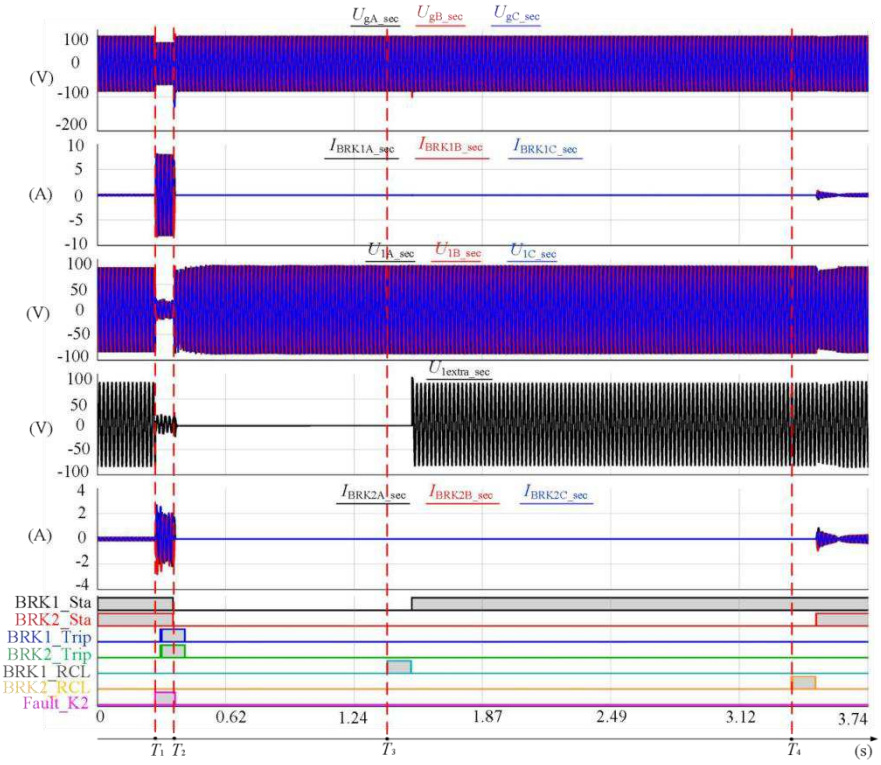

Figure 16. Voltage and current trends at Protection 1 and Protection 2 during the K2 fault on the feeder under the high-generation–high-load mode.

Case 3: Distributed energy storage (DES) in service, low-flow–high-load mode, ABN phase-to-ground fault at K3

In the low-flow–high-load mode, all DES units are in operation. An ABN phase-to-ground fault is simulated at point K3. Before the fault, the DES units operate under coordinated voltage control. Line 2 transmits 1.04 MW active power and –0.58 MVar reactive power, meaning the Region 2 network absorbs approximately 1.04 MW active power from the substation and feeds back 0.58 MVar reactive power.

As shown in Figure 17, at T1, a BCN fault occurs at K3. Differential protection at BRK3 (Protection 3) and BRK4 (Protection 4) operates. After 88 ms, at T2, BRK3 and BRK4 trip, forming an island in Region 2. Initially, the island experiences voltage and frequency drops. The voltage coordinated control strategy quickly acts to maintain the island voltage at around 0.98 pu. As the frequency decreases, the frequency deviation control strategy is activated to gradually restore the island frequency to the rated value.

At T3, Protection 3 recloses BRK3, and Protection 4 begins comparing the line-extracted voltage with node voltages. With the frequency deviation control gradually bringing the island

frequency to approximately 0.991 pu, the synchronization condition for Protection 4 is met. At T4, Protection 4 successfully recloses BRK4, and Region 2 island is restored to the grid. The total duration from fault occurrence to island restoration is approximately 2052 ms.

It should be noted that while BESS2 and BESS3 perform island self-healing, BESS1 remains grid-connected. Its voltage coordinated control remains effective, and the voltage at Node 1 stays nearly unchanged before and after fault isolation.

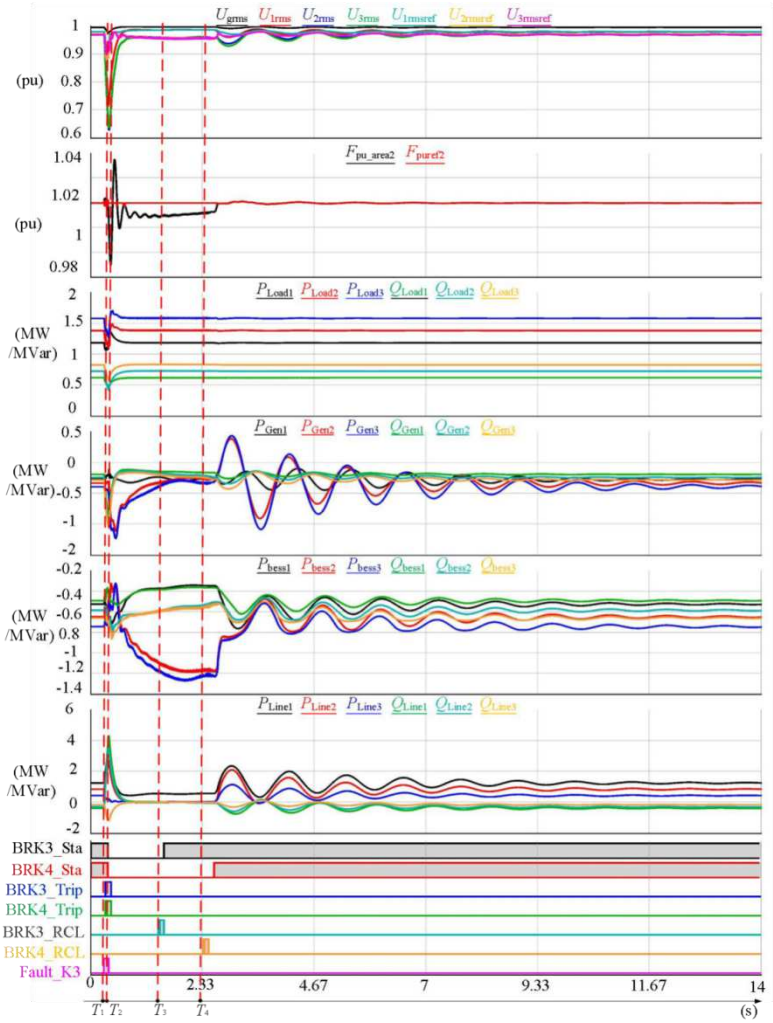

Figure 17. Node voltage and power variations under K3 fault on the feeder during low-flow, heavy-load conditions

The secondary voltage and current at Protection 3, and the secondary voltage, extracted voltage, and current at Protection 4, are shown in Figure 18. At T1, a K3 fault occurs on the feeder, and Protections 3 and 4 detect the increased fault current. The line differential protection operates and sends trip commands to BRK3 and BRK4. At T2, the circuit breakers on both sides of Line 2 are opened. By T3, Protection 3 recloses, closing BRK3 and restoring voltage to the line. Protection 4

detects the line's extracted voltage and begins the synchronization check. By T4, the synchronization condition is met, Protection 4 recloses successfully, closing BRK4, and the feeder is restored to grid operation.

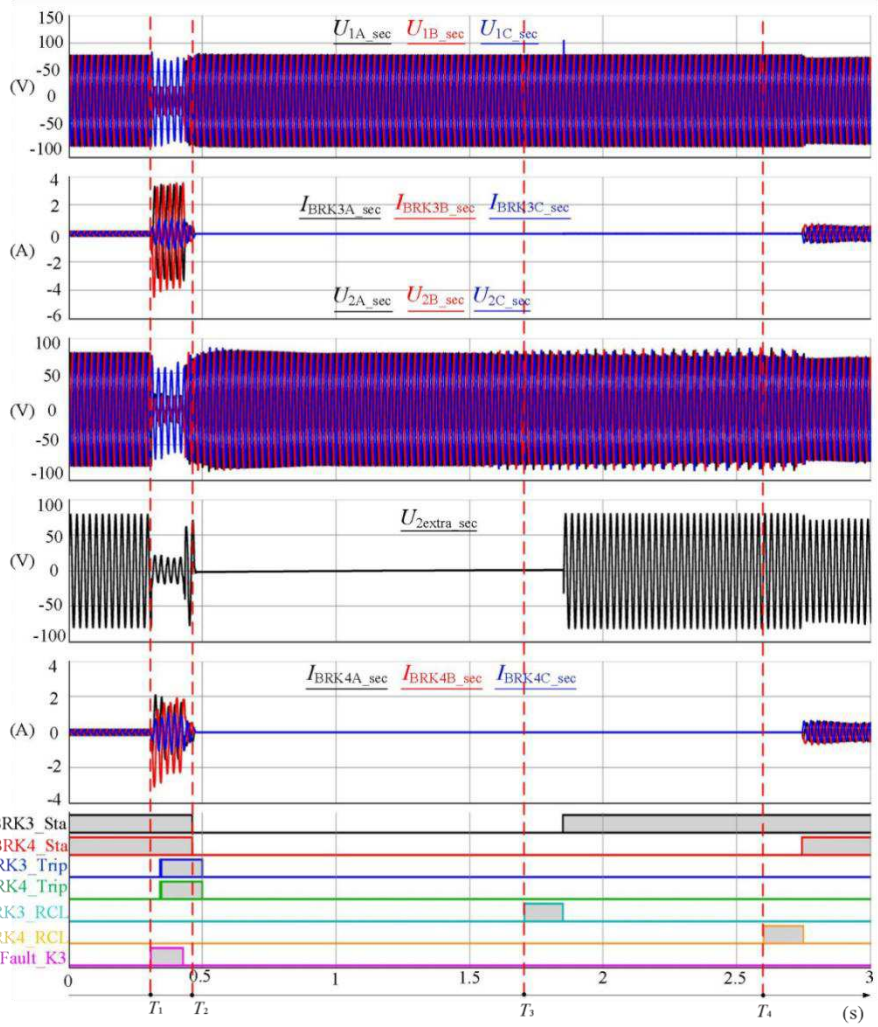

Figure 18. Voltage and current trends of Protection 3 and Protection 4 during the K3 fault on the feeder under low-flow–high-load conditions.

Case 4: Distributed Energy Storage in Operation, High-Generation–Low-Load Mode, K4 BC Fault

In the high-generation–low-load mode, the distributed energy storage (DES) group is active. A BC fault is simulated at point K4, lasting 100 ms. Prior to the fault, the DES units operate under coordinated voltage control. The power on Line 3 is -0.37 MW active and 0.05 MVar reactive, meaning that Area 3 feeds 0.37 MW of active power back to the main substation while drawing 0.05 MVar of reactive power. The voltage and power variations at each node during the K4 fault under this case are shown in Figure 19.

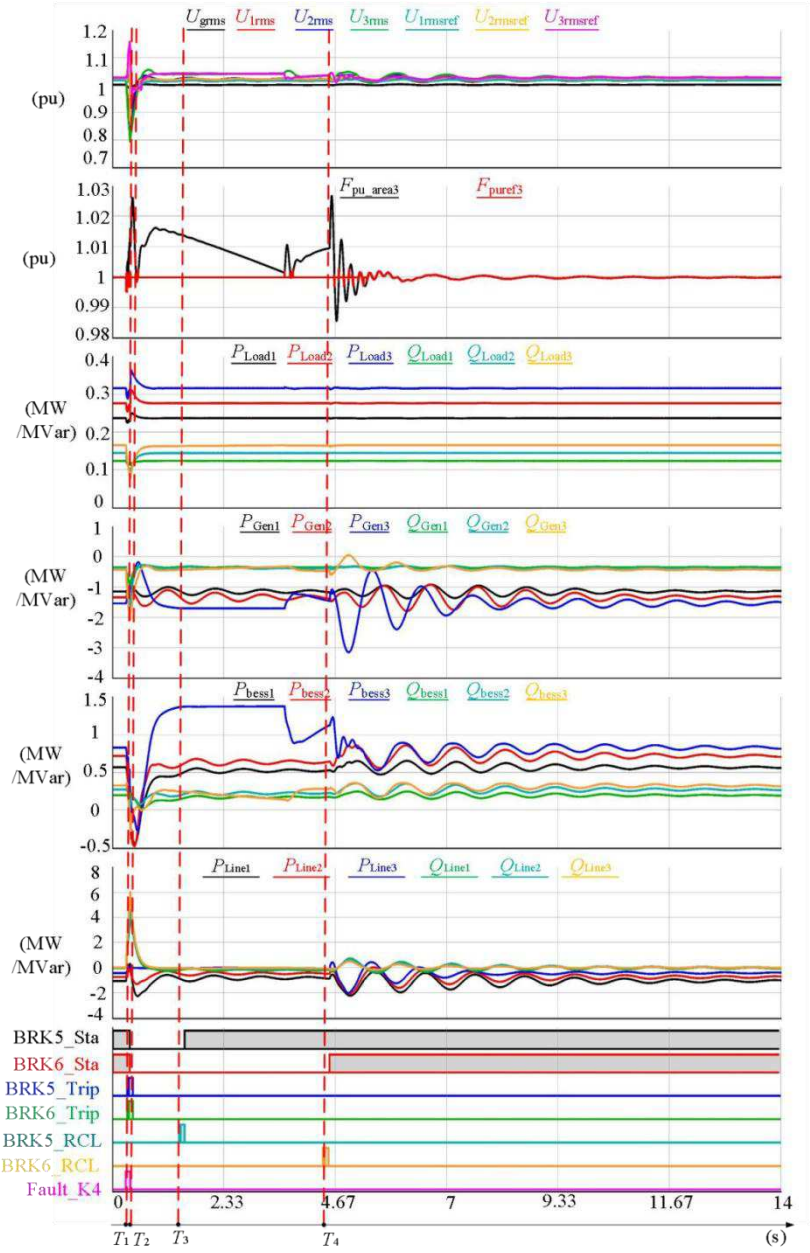

Figure 19. Node Voltage and Power Variation Trends during K4 Fault on the Feeder under High-Generation–Low-Load Mode

From the simulation results shown in Figure 19, at T1, a BC fault occurs at K4. Differential protection at BRK5 (Protection 5) and BRK6 (Protection 6) is triggered. After 88 ms, at T2, BRK5 and BRK6 trip, forming an islanded feeder in Area 3. Due to excess power in the islanded network, both voltage and frequency rise, but the distributed energy storage (DES) quickly regulates the island voltage from 1.015 pu back to its rated value. Simultaneously, the frequency deviation control strategy is activated to bring the island frequency to its nominal value. As the frequency approaches around 1.002 pu, the frequency control loop is temporarily frozen because the control trigger

condition is no longer met, causing a brief frequency spike. The frequency control strategy is then reactivated for a second round of regulation. At T4, the synchronization conditions for Protection 6 are satisfied, the reclosing succeeds, and the Area 3 island reconnects to the grid. The total duration from fault occurrence to island restoration is approximately 4261 ms. Afterwards, the DES group resumes its coordinated voltage control mode in the grid. During the islanded operation of BESS3, BESS1 and BESS2 remain connected to the grid, and their voltage coordination control remains effective.

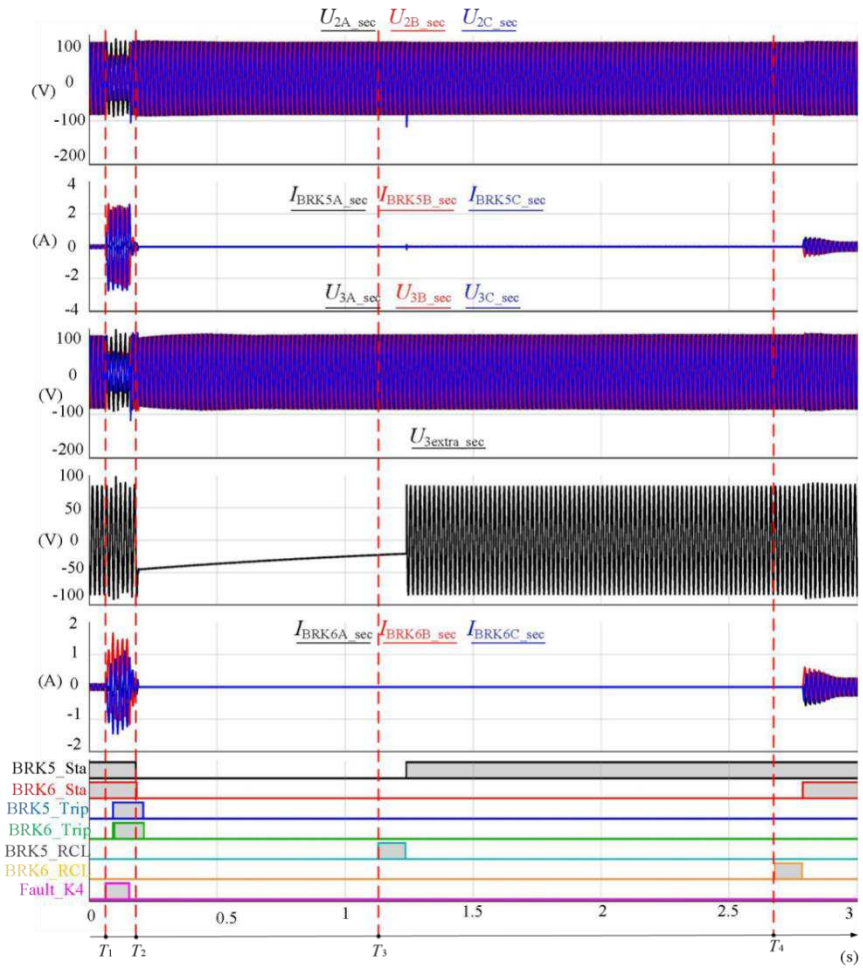

Figure 20. The voltage and current variations at Protection 5 and Protection 6 during the K4 BC fault on the feeder under the high-generation–low-load mode

The secondary voltage and current at Protection 5, and the secondary voltage, extracted voltage, and current at Protection 6 are shown in Figure 20. The operating logic of Protection 5 and Protection 6 is the same as that of Protection 1 and Protection 2 during the K2 fault and will not be repeated here.

4 Conclusions

This paper proposes a coordinated voltage control method based on an improved droop control and a frequency control method based on a dual-hysteresis comparator strategy, applied to distributed energy storage (DES) cluster control. The approach addresses issues of feeder overvoltage and power interruptions caused by feeder backfeeding. The method consists of a voltage coordination control strategy and a frequency deviation control strategy. The voltage coordination strategy is effective under both grid-connected and islanded conditions, while the frequency coordination strategy is only activated when the feeder is islanded.

Firstly, the voltage distribution characteristics of the feeder are analyzed. Then, a slope is introduced into the voltage control loop of DES, and a coordinated voltage control method based on improved droop control is proposed. This method considers both DES capacity and line impedance, establishing a principle for DES slope setting to control voltages at all feeder nodes. This voltage control approach does not rely on communication systems or require slope updates, showing strong adaptability under both grid-connected and islanded conditions. It can suppress voltage fluctuations across all nodes during grid-connected operation and maintain stable voltages during feeder islanding.

Next, enable control is introduced into the frequency control loop, and a frequency deviation control method based on a dual-hysteresis comparator is proposed. The method uses upward and downward hysteresis comparators to detect frequency deviations in different directions. Depending on the thresholds, the DES frequency deviation control loop is activated or frozen. This gives the frequency control curve a hysteresis characteristic, providing strong anti-interference capability against frequency deviations caused by power fluctuations in grid-connected mode. It also enables DES units to accurately identify feeder islanding without communication and activate the frequency deviation control loop in a timely manner, stabilizing the feeder island frequency.

Through reclosing or automatic restoration, the method enables fast self-healing of feeder faults. Finally, to validate the proposed method, a real-time closed-loop simulation platform incorporating DES models and line protection devices was built, conducting full-process simulation of voltage coordination control and feeder island frequency stabilization. Simulation results confirm the effectiveness of the proposed approach.

This study further highlights the role of distributed energy storage in power systems, which will facilitate its broader application in modern grids.

5 Funding Declaration

This work was supported by the Jiangxi Province Early-Career Young Scientific and Technological Talent Cultivation Program (Grant No. 20262BEJ730095).

6 Ethics Approval

This study did not involve human participants or animals, and therefore ethical approval was not required.

7 References

[1] Zhang Z, Zhang H, Zhou L, et al. Island Partition Strategy Based on Entropy Method-Set Pair Analysis for Microgrids[J]. IEEE Access, 2025.

[2] Xu B, Paduani V D, Xiao Q, et al. Under-Frequency Load Shedding for Power Reserve Management in Islanded Microgrids[J]. IEEE Transactions on Smart Grid, 2024, 15(5): 4662.

[3] Chen Q, Sanaullah K, Tahir A, et al. Adaptive islanding strategy of sustainable distribution system for post-restoration failures[J]. CSEE Journal of Power and Energy Systems, 2022, 9(4): 1517-1531.

[4] Sanaullah K, Xia M, Hussain M, et al. Optimal islanding for restoration of power distribution systems using prim's MST algorithm[J]. CSEE Journal of Power and Energy Systems, 2020, 8(2): 599-608.

[5] Shen F, Wu Q, Xue Y. Review of service restoration for distribution networks[J]. Journal of Modern Power Systems and Clean Energy, 2019, 8(1): 1-14.

[6] Arefifar S A, Alam M S, Hamadi A. A review on self-healing in modern power distribution systems[J]. Journal of Modern Power Systems and Clean Energy, 2023, 11(6): 1719-1733.

[7] Cho S C , Lee G S .A local control of interlinking DC/DC converters in DC microgrid clusters for global power sharing[J].IET Conference Proceedings, 2025, 2024(29):285-290.

[8] You Z , Wang H , Song Z ,et al.Photovoltaic consumption strategy of distribution network considering carbon emission and user experience[J].International Journal of Power and Energy Conversion, 2025, 16(1):38-61.

[9] Saaklayen M A, Liang X, Faried S O, et al. Soft open point-based service restoration coordinated with distributed generation in distribution networks[J]. IEEE Transactions on Industry Applications, 2023, 60(2): 2554-2566.

[10] Xia T , Zhan S , Zhou Y ,et al.Capacity optimisation configuration of active distribution network under distributed photovoltaic access[J].International Journal of Energy Technology and Policy, 2025, 20(1-2):20-35.

[11] Kamberi K , Shaliu D , Elo M ,et al.Hosting capacity calculation of photovoltaic penetration in a closed loop distribution network: a case study[J].IET Conference Proceedings, 2025, 2024(29):113-118.

[12] Khan M W, Li G, Wang K, et al. Optimal control and communication strategies in multi-energy generation grid[J]. IEEE Communications Surveys & Tutorials, 2023, 25(4): 2599-2653.
[13] Batool M , Hassan W , Lu D C .Review of Advanced Control Strategies for Isolated DC–DC Converters in DC Microgrids[J].Access, IEEE, 2025, 13(000):103137-103154.
[14] Paz P , Hebner R , Gattozzi A ,et al.Series Arc Faults in a Megawatt-Level DC Microgrid[J].Power Delivery, IEEE Transactions on, 2025, 40(5):2832-2839.
[15] Feng J, Yu T, Zhang K, et al. Integration of multi-agent systems and artificial intelligence in self-healing subway power supply systems: Advancements in fault diagnosis, isolation, and recovery[J]. Processes, 2025, 13(4): 1144.
[16] Demirel G , Grafenhorst S , Frderer K ,et al.Impact and Integration of Mini Photovoltaic Systems on Electric Power Distribution Grids[J].Lecture Notes in Computer Science, 2025:247-265.
[17] Zhai D , Ye W , Ma M ,et al.Simulation model of active distribution network lines with high proportion distributed photovoltaic energy storage access[J].International Journal of Renewable Energy Development, 2025, 14(2):290-298.
[18] Yang Z, Han J, Li L, et al. Research of islanding operation and fault recovery strategies of distribution network considering uncertainty of new energy[J]. Electronics, 2023, 12(20): 4230.
[19] Suharso P , Wijaksono U , Praja B I .Load Flow Optimization on the UP3 Singkawang Sui Baru Feeder Distribution Network to Minimize Power Losses[J].2024 International Conference on Technology and Policy in Energy and Electric Power, 2024:307-312.
[20] Khatiwada R , Bajracharya T R , Khan S .Improving the Energy Efficiency of a Power Distribution Network by Loss Reduction: A Case Study in Rural 11 Kv Feeder[J].Journal of Advanced College of Engineering and Management, 2024, 9:339-349.
[21] Pragati A, Mishra M, Rout P K, et al. A comprehensive survey of HVDC protection system: fault analysis, methodology, issues, challenges, and future perspective[J]. Energies, 2023, 16(11): 4413.
[22] Anderson A A, Vadari S V, Barr J L, et al. Introducing the 9500 node distribution test system to support advanced power applications: An operations-focused approach[R]. Pacific Northwest National Laboratory (PNNL), Richland, WA (United States), 2022.
[23] Alishov R , Bhatt S , Dinkel D ,et al.Active Power Feeder: The New Medium-Voltage Power Supply Solution With Huge Benefits in Power Quality and Electric Arc Furnace Regulation[J].AISTech 2024 Proceedings, 2024:419-423.
[24] Fattahi J .Data-Driven Fault Recovery With Software-Defined Smart Transmission Grids[J].IEEE Access, 2024, 12:183354-183368.
[25] Zhou Z , Xia Y , Wen Y ,et al.Distribution Feeder Fault Detection Method Considering Transient Frequency Response of Distributed Power Supply[J].IET Smart Grid, 2025, 8(1).
[26] Ibrahim A H M, Sadanandan S K, Ghaoud T, et al. Incipient fault detection in power distribution networks: review, analysis, challenges and future directions[J]. IEEE Access, 2024.
[27] Naidu R D , Khatod D K , Das B .Estimation of Distribution Network Feeder Parameters: A Linearized Approach[J].2024 IEEE International Conference on Smart Power Control and Renewable Energy , 2024:1-5.
[28] Yang J , Ye H , Wang Y ,et al. Mechanism and Methods for Fault Recovery of Grid-Forming Inverter by Graphical Illustration[J].Power Systems, IEEE Transactions on, 2025, 40(2):1973-1976.

[29] Arjomandi-Nezhad A , Guo Y , Pal B C ,et al.Modeling Fault Recovery and Transient Stability of Grid-Forming Converters Equipped With Current Reference Limitation[J].Energy Conversion, IEEE Transactions on, 2025, 40(2):1140-1152.

[30] Rkmez M , Kallese C , Bendtsen J D ,et al.Optimizing Photovoltaic Panel Quantity for Water Distribution Networks[J].Control Systems Technology, IEEE Transactions on, 2025, 33(5):1727-1742.